

# PROCEEDINGS OF SPIE

[SPIEDigitallibrary.org/conference-proceedings-of-spie](https://www.spiedigitallibrary.org/conference-proceedings-of-spie)

## Prehistoric beaten-copper cranium

Schulz, Georg, Nicklisch, Nicole, Rojo Guerra, Manuel, Müller, Bert, Alt, Kurt

Georg Schulz, Nicole Nicklisch, Manuel Rojo Guerra, Bert Müller, Kurt W. Alt, "Prehistoric beaten-copper cranium," Proc. SPIE 11840, Developments in X-Ray Tomography XIII, 1184006 (4 October 2021); doi: 10.1117/12.2594279

**SPIE.**

Event: SPIE Optical Engineering + Applications, 2021, San Diego, California, United States

# Prehistoric beaten-copper cranium

Georg Schulz<sup>a,b</sup>, Nicole Nicklisch<sup>c</sup>, Manuel Rojo Guerra<sup>d</sup>, Bert Müller<sup>a,e</sup>, Kurt W. Alt<sup>c,f</sup>

<sup>a</sup>Biomaterials Science Center, Department of Biomedical Engineering, University of Basel,  
4123 Allschwil, Switzerland;

<sup>b</sup>Core Facility Micro- and Nanotomography, Department of Biomedical Engineering,  
University of Basel, 4123 Allschwil, Switzerland;

<sup>c</sup>Center of Natural and Cultural Human History, Danube Private University, 3500 Krems, Austria;

<sup>d</sup>Department of Prehistory and Archaeology, Faculty of Philosophy and Letters,  
Valladolid University, 47002 Valladolid, Spain;

<sup>e</sup>Biomaterials Science Center, Department of Clinical Research, University Hospital Basel,  
4031 Basel, Switzerland;

<sup>f</sup>Integrative Prehistory and Archaeological Science, Department of Environmental Sciences, University of  
Basel, 4056 Basel, Switzerland

## ABSTRACT

Laboratory-based X-ray microtomography has become indispensable for imaging unique objects. Especially for large objects including the human skull, laboratory-based devices have the big advantage of having a reasonable field of view of up to a dozen of centimeters in comparison to synchrotron-radiation based microtomography with a typical field of view smaller than a centimeter. Using a nanotom® m, we investigated a prehistoric case of a ‘beaten-copper’ cranium from around 5,000 BCE discovered at the site of Els Trocs in the Spanish pyrenees. The skull of an approximately five-year-old child (ET1/CET1) shows distinct impressions of the cerebral convolutions (gyri cerebri) on the inner surface of the frontal, parietal and occipital bone. These changes are visually reminiscent of beaten-copper and are associated with chronically increased intracranial pressure, which may have various causes.

**Keywords:** Lab-based X-ray source, hard X-ray microtomography, beaten-copper phenomenon, intercranial pressure, human cranium, ancient skull

## 1. INTRODUCTION

In the Spanish Pyrenees, there are numerous caves that were not only used as shelters and seasonal dwellings in prehistoric times, but also as burial sites. In most cases, no complete skeletons are found there, but only isolated bone fragments scattered throughout the cave [1]. This is partly also true for the Els Trocs cave (Sant Feliu de Verim Bisaurri, Huesca, Spain), located on the southern slope of a karst hill at about 1500 m above sea level [2]. It is characterised by its excellent geographical and climatic position, as the plateau is suitable for pasture in the summer months. A network of paths can be identified that have been used since the Neolithic period. Numerous archaeological findings suggest that the cave was used in spring and summer as part of a seasonal transhumance [2, 3]. Between 2009 and 2019, several excavation campaigns took place in which more than 1200 individual human bones were found in the cave chamber. Due to the constantly cool and humid environment inside the cave, the structural bone preservation is excellent. An osteological analysis of the single bone fragments enabled the identification of a minimum number of 19 individuals [4]. The individuals date to different phases of occupation of the caves, ranging from the Neolithic to modern times.

Conventional X-ray microtomography ( $\mu$ CT) is a well established, non-destructive imaging technique for volumetric visualization of tissue morphology in the biomedical field [5-9]. Due to the high flux available at synchrotron radiation facilities, synchrotron radiation-based  $\mu$ CT (SR $\mu$ CT) allows for superior image quality with respect to contrast and spatial resolution [10, 11]. One of the disadvantages of SR $\mu$ CT is the limited beamtime available. Secondly, the beam size at recent

synchrotron radiation facilities of around 10 mm only allows the visualization of smaller objects. Therefore,  $\mu$ CT became more interesting for the visualization of larger human body parts [12, 13] or unique, archaeological objects [4, 14, 15]. The Core Facility ‘Micro- and Nanotomography’ (MiNa) at the Department of Biomedical Engineering of the University of Basel operates two state-of-the-art X-ray microtomography systems, a Skyscan 1275 (Bruker microCT, Kontich, Belgium) and a nanotom® m (Waygate Technologies, Wunstorf, Germany). The desktop system Skyscan 1275 is mainly used for investigations of low Z materials [9], or for student courses due to its user-friendliness. Due to the 180 kV X-ray source and the relatively large source-to-detector distance of 60 cm, the nanotom® m can scan high Z materials or objects with diameters of up to 35 cm.

## 2. MATERIAL AND METHODS

### 2.1 Excavation at ElsTrocs

The individual ET1/CET1 examined in this study dates to the oldest phase around 5300 BCE [16]. It is a child whose skull could be reconstructed from the individual bones almost completely (Fig. 1 left). Postcranial bones could not be assigned. Based on the developmental stage of the teeth [17], the age at death can be estimated at about 5 years. The internal tabula of the frontal, parietal and occipital bones shows distinct impressions of the cerebral convolutions (gyri cerebri). These changes are visually reminiscent of beaten-copper and are associated with chronically increased intracranial pressure, which may have various causes [18]. In this case, the beaten-copper pattern could also be observed in other children of different ages. A square sample was taken from the frontal bone, which was used for palaeogenetic studies and isotope analyses for dietary reconstruction.

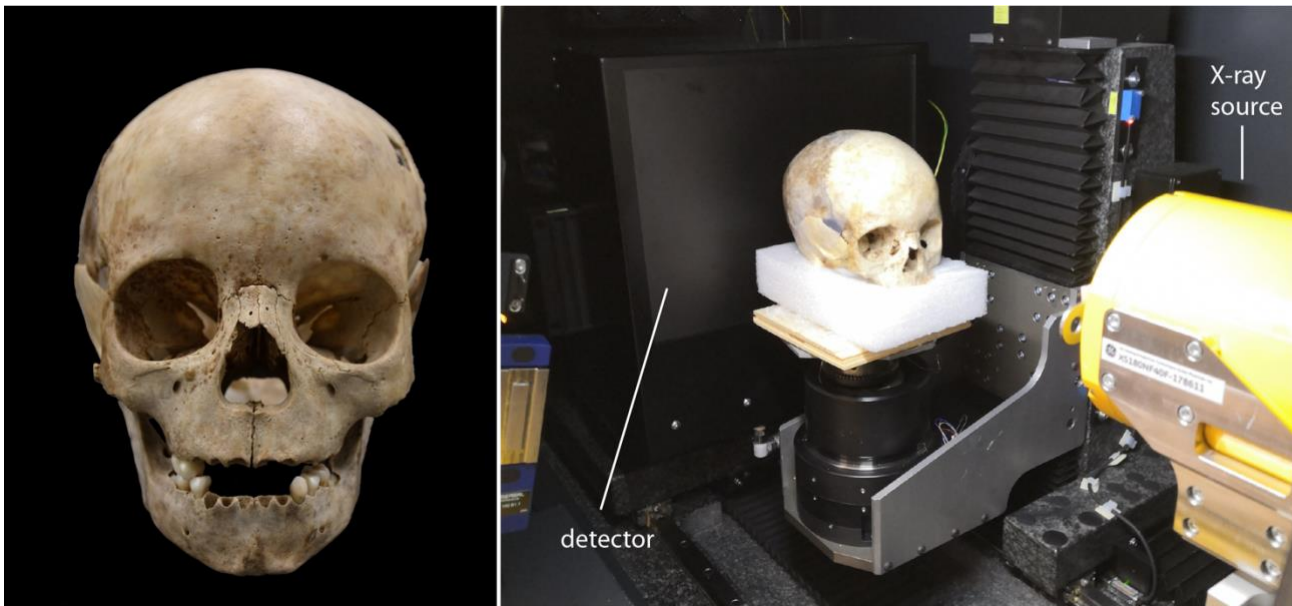


Figure 1. Frontal view of the reconstructed skull of individual ET1/CET1 (left) and a photograph of the skull within microtomography system just before the scan.

### 2.2 X-ray microtomography

The investigation was performed with a nanotom® m (Waygate Technologies, Wunstorf, Germany). The 60 cm distance between source and detector and a horizontal shift of the detector (3,072 pixels  $\times$  2,400 pixels) allows visualizing specimens up to 35 cm in diameter. The inside of the scanner including the object is shown in Fig. 1. First an overview scan of the frontal, parietal and occipital bones was performed followed by a higher resolution scan of the frontal bone. For the higher resolution scan, the frontal bone was removed from the skull. Both scans were acquired with an acceleration voltage of 150 kV and a

beam current of  $60 \mu\text{A}$ . In order to increase the mean energy a Cu-filter with  $0.25 \text{ mm}$  thickness was introduced. For both scans 2000 radiographs at equiangular positions over  $360^\circ$  were acquired. The overview scan was recorded with a pixel size of  $68 \mu\text{m}$  with an exposure time of  $12 \text{ s}$  for each projection resulting in a total scan duration of  $8 \text{ h}$  and  $20 \text{ min}$ . The higher resolution scan had a pixel size of  $40 \mu\text{m}$  with an exposure time of  $10 \text{ s}$  and a total scan time of  $6 \text{ h}$  and  $40 \text{ min}$ .

### 2.3 Skull thickness determination

The determination of the skull thickness distribution was performed with MATLAB. To determine the skull thickness distribution, the following steps were performed (Fig. 2): After binarization of the data set, the trabecular holes were filled (imfill(...,'holes') function) and gaps were closed (imclose(...,strel('disk',50) function). Then a 3D distance transform of the data set was calculated (bwdist function) [19]. The values located on the centerline of the distance transform (bwmorph(...,'skel',Inf) function) are then associated with half of the skull thicknesses.

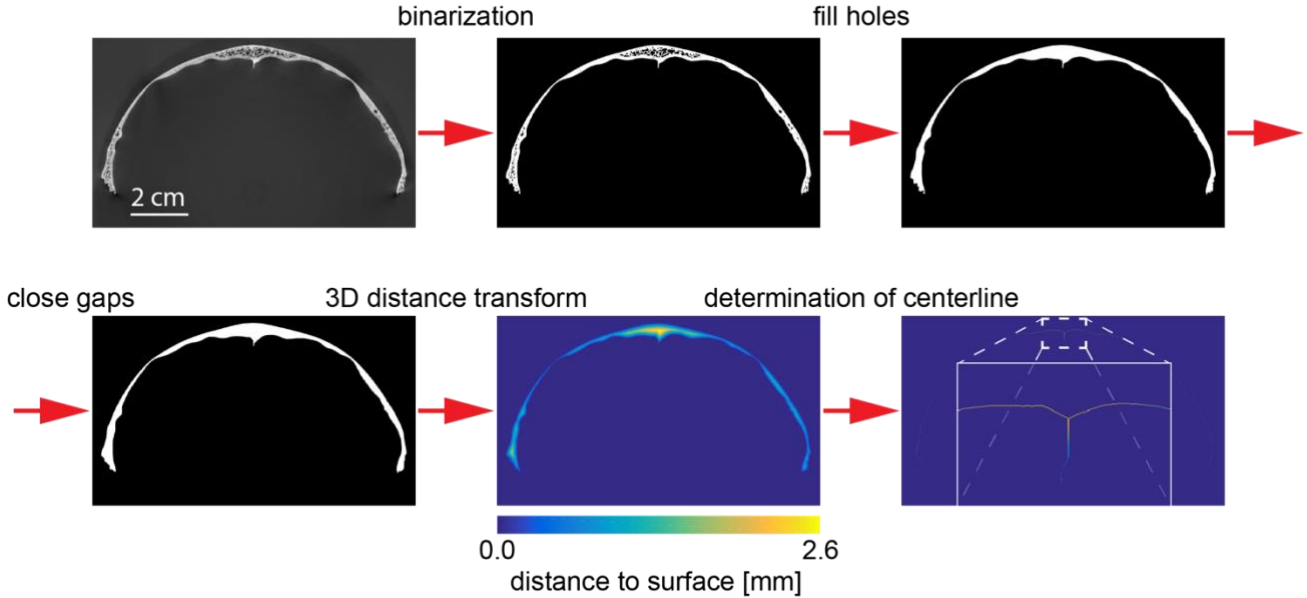


Figure 2. Schematic representation of the determination of the skull thickness distribution.

## 3. RESULTS & DISCUSSION

The reconstructed skull containing the frontal, occipital and the right parietal bones were first imaged with a pixel size of  $68 \mu\text{m}$ . The chosen spatial resolution is related to the large size of the object. Due to the high absorption of the object a relatively high acceleration voltage had to be set and a Cu-filter introduced in order to increase the mean photon energy. Such scans could not be performed in the Skyscan 1275 with its maximum acceleration voltage of  $100 \text{ kV}$ . A second challenge was the fixation of the object. In order to avoid a damage to the skull, we decided not to use glue for fixation. The skull was fixed in foam material which was trimmed with respect to the shape of the object. The skull fitted in the cavities of the foam material and prevented any movements of the skull during the measurements.

The 3D volume rendering of the data set (front and both side views), is shown in Fig. 3. The absent left parietal bone enables a view of the inner surface of the right parietal bone. On the inner surface distinct impressions are visible. The phenomenon is called beaten-copper in relation to the pattern in hand-beaten copper objects like bowls and dishes. The irregularities are induced by raised intracranial pressure. Potential pathologies are craniosynostosis, obstructive hydrocephalus, hypophosphatasia or the Marfan syndrome. After reducing the size of the object by removing the occipital and the right parietal bones the pixel size of the scan could be reduced to  $40 \mu\text{m}$ . The front and back views of the 3D rendering of this higher resolution data set are shown in Fig. 4. The inner surface of the frontal bone again shows the mentioned impressions. In order

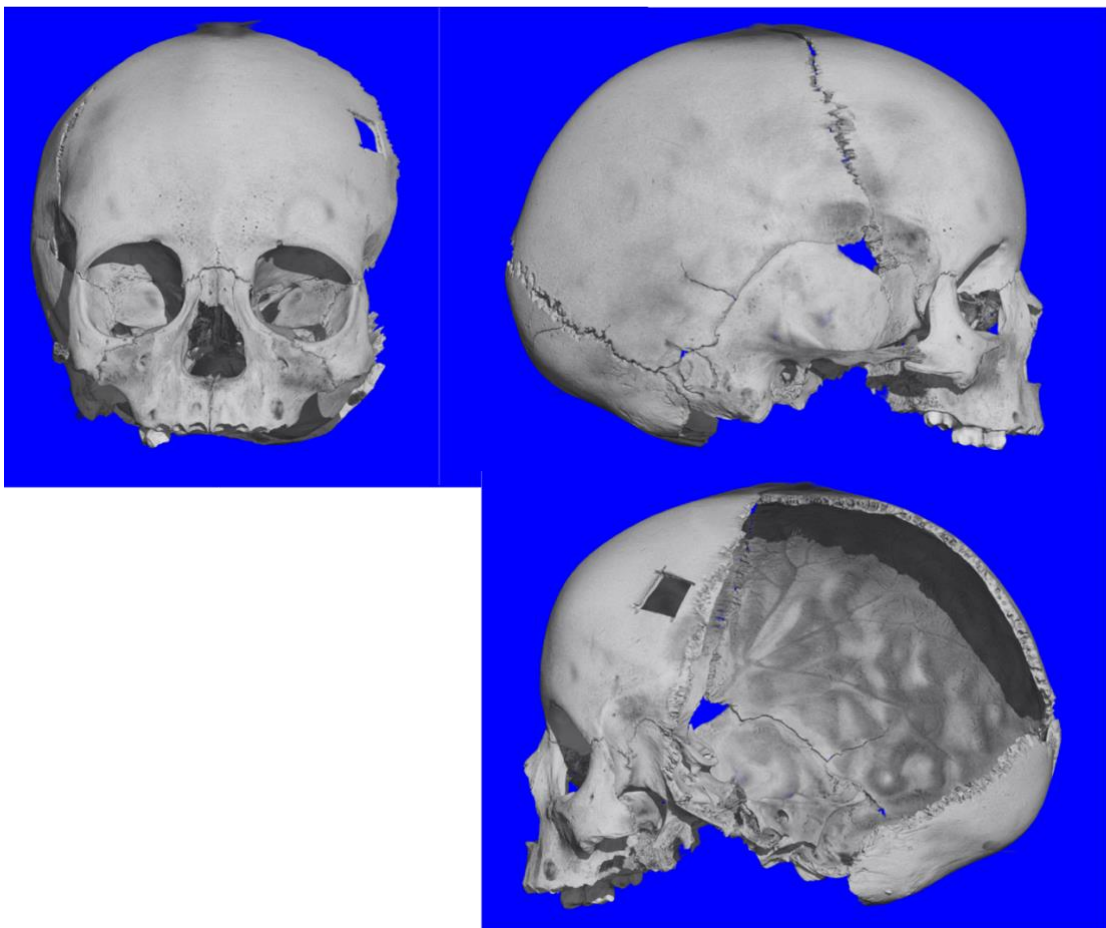


Figure 3. Frontal and two lateral views of a 3D rendering of the reconstructed skull. The missing left parietal bone allows a look on the inner surface of the right parietal bone indicating the interesting features.

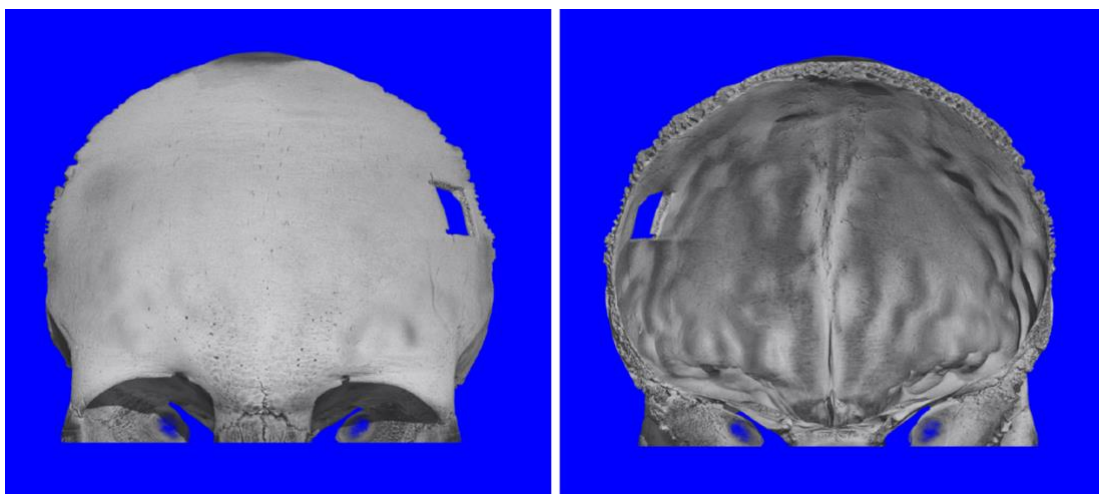


Figure 4. Frontal and backside view of the higher resolved data set of the frontal bone.

to quantify the visual inspection, a skull thickness distribution was determined following the steps shown in Fig. 2. A color-coded 3D rendering of the skull thickness distribution is shown in Fig. 5. The thicknesses vary between 1 and 4 mm and the figure clearly shows the permanent alteration of the thicknesses related to the beaten-copper phenomenon.

The observed patterns could also be found in other children of different ages of the excavation. Since hydrocephalus and craniosynostosis can be ruled out, an infection of the meninges would be conceivable. In view of the presumably practiced transhumance, an adaptive reaction to the differences in altitude would also be a possible explanation. The investigations on this question are still ongoing.

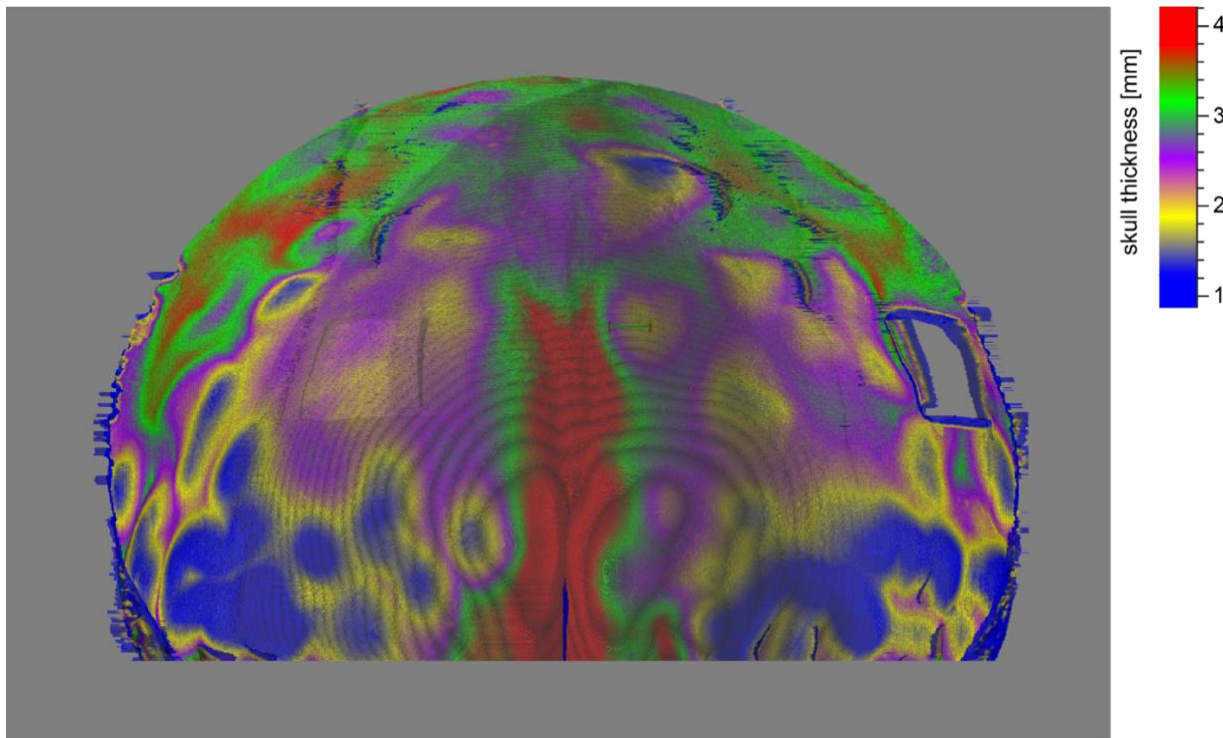


Figure 5. Skull thickness distribution in the frontal bone.

#### 4. CONCLUSION

The big advantage of laboratory-based microtomography is the possibility to investigate decimeter-sized archeological objects on the microscopic level. Our study revealed the beaten copper phenomenon of a prehistoric skull of a 5-year-old child induced by chronically increased intracranial pressure. Using the 3D distance transform of the data set, skull thickness distribution was determined. The determination of the skull thickness distribution using distance transform could be of potential interest to diagnose beaten copper phenomenon using clinical CT scan.

#### ACKNOWLEDGEMENTS

The authors acknowledge financial support of the Swiss National Science Foundation (SNSF) in the frame of the R'equip initiative (133802) and from the German Research Foundation (AL 287/14-1). Financial support for several excavation campaigns in Spain was provided by the Danube Private University in Krems, Austria.

## REFERENCES

- [1] R. Garrido-Pena, M. Rojo-Guerra, C. Tejedor-Rodríguez, and I. García-Martínez de Lagrán, [Las máscaras de la muerte: ritos funerarios en el Neolítico de la Península Ibérica], Madrid(2012).
- [2] M. Rojo Guerra, L. Peña-Chocarro, J. Royo-Guillén, C. Tejedor-Rodríguez, Í. García-Martínez-de-Lagrán, H. Arcusa Magallón, R. Garrido Pena, M. Moreno, N. Mazzucco, J. Gibaja, D. Ortega, B. Kromer, and K. Alt, "Pastores trashumantes del Neolítico Antiguo en un entorno de alta montaña: Secuencia crono-cultural de la Cova de Els Trocs (San Faliú de Veri, Huesca)," *Boletín del seminario de estudios de arte y arqueología*, 79, 9-55 (2013).
- [3] C. Lancelotti, A. Balbo, M. Madella, E. Iriarte, M. Rojo-Guerra, J. Royo, C. Tejedor, R. Garrido, I. García, H. Arcusa, G. Pérez Jordà, and L. Peña-Chocarro, "The missing crop: investigating the use of grasses at Els Trocs, a Neolithic cave site in the Pyrenees (1564 m asl)," *Journal of Archaeological Science*, 42, 456-466 (2014).
- [4] K. W. Alt, C. Tejedor Rodríguez, N. Nicklisch, D. Roth, A. Szécsényi Nagy, C. Knipper, S. Lindauer, P. Held, I. García Martínez de Lagrán, G. Schulz, T. Schuerch, F. Thieringer, P. Brantner, G. Brandt, N. Israel, H. Arcusa Magallón, C. Meyer, B. G. Mende, F. Enzmann, V. Dresely, F. Ramsthaler, J. I. Royo Guillén, E. Scheurer, E. López Montalvo, R. Garrido Pena, S. L. Pichler, and M. A. Rojo Guerra, "A massacre of early Neolithic farmers in the high Pyrenees at Els Trocs, Spain," *Scientific Reports*, 10, 2131 (2020).
- [5] F. Bornert, F. Clauss, G. Hua, Y. Idoux-Gillet, L. Keller, G. Fernandez De Grado, D. Offner, R. Smaida, Q. Wagner, F. Fioretti, S. Kuchler-Bopp, G. Schulz, W. Wenzel, L. Gentile, L. Risser, B. Müller, O. Huck, and N. Benkirane-Jessel, "Mechanistic illustration: How newly formed blood vessels stopped by the mineral blocks of bone substitutes can be avoided by using innovative combined therapeutics," *Biomedicines*, 9, 952 (2021).
- [6] C. Stutz, F. Clauss, O. Huck, G. Schulz, N. Benkirane-Jessel, F. Bornert, S. Kuchler-Bopp, and M. Strub, "Eruption of bioengineered teeth: A new approach based on a polycaprolactone biomembrane," *Nanomaterials*, 11, 1315 (2021).
- [7] M. Sacher, G. Schulz, H. Deyhle, K. Jäger, and B. Müller, "Accuracy of commercial intraoral scanners," *Journal of Medical Imaging*, 8, 035501 (2021).
- [8] W. Kuo, N. A. Le, B. Spangler, R. H. Wenger, A. Kipar, U. Hetzel, G. Schulz, B. Müller, and V. Kurtcuoglu, "Simultaneous three-dimensional vascular and tubular imaging of whole mouse kidneys with X-ray  $\mu$ CT," *Microscopy and Microanalysis*, 26, 731-740 (2020).
- [9] M. Osterwalder, J. S. Bolten, G. Rodgers, M. Humbel, G. Schulz, C. Tanner, J. Huwyler, and J. Müller, "Hard X-ray microtomography of zebrafish larvae," *Proceedings of SPIE*, 11886, 1188614 (2021).
- [10] E. Cörek, G. Rodgers, S. Siegrist, T. Einfalt, P. Detampel, C. M. Schlepütz, S. Sieber, P. Fluder, G. Schulz, H. Unterweger, C. Alexiou, B. Müller, M. Puchkov, and J. Huwyler, "Shedding light on metal-based nanoparticles in zebrafish by computed tomography with micrometer resolution," *Small*, 16, 2000746 (2020).
- [11] G. Rodgers, G. Schulz, W. Kuo, M. Scheel, V. Kurtcuoglu, T. Weitkamp, B. Müller, and C. Tanner, "Non-rigid registration to determine strain fields during mouse brain fixation and embedding," *Proceedings of SPIE*, 11586, 115860I (2021).
- [12] G. Schulz, C. Götz, H. Deyhle, M. Müller-Gerbl, I. Zanette, M.-C. Zdora, A. Khimchenko, P. Thalmann, A. Rack, and B. Müller, "Hierarchical imaging of the human knee," *Proceedings of SPIE*, 9967, 99670R (2016).
- [13] M. Dalstra, G. Schulz, D. Dagassan-Berndt, C. Verna, M. Müller-Gerbl, and B. Müller, "Hard X-ray microtomography of a human head post-mortem as a gold standard to compare X-ray modalities," *Proceedings of SPIE*, 9967, 99670P (2016).
- [14] B. Mennecart, C. Guignard, L. Dziomber, G. Schulz, B. Müller, and L. Costeur, "Allometric and phylogenetic aspects of stapes morphology in Ruminantia (Mammalia, Artiodactyla)," *Frontiers in Earth Science*, 8, 176 (2020).
- [15] L. Costeur, B. Mennecart, B. Müller, and G. Schulz, "Observations on the scaling relationship between bony labyrinth, skull size and body mass in ruminants," *Proceedings of SPIE*, 11113, 111130Q (2019).
- [16] A. Szécsényi-Nagy, C. Roth, G. Brandt, C. Rihuete-Herrada, C. Tejedor-Rodríguez, P. Held, I. García-Martínez-de-Lagrán, H. Arcusa Magallón, S. Zesch, C. Knipper, E. Bánffy, S. Friederich, H. Meller, P. Bueno Ramírez, R. Barroso Bermejo, R. de Balbín Behrmann, A. M. Herrero-Corral, R. Flores Fernández, C. Alonso Fernández, J. Jiménez Echevarria, L. Rindlisbacher, C. Oliart, M. I. Fregeiro, I. Soriano, O. Vicente, R. Micó, V. Lull, J. Soler Díaz, J. A. López Padilla, C. Roca de Togores Muñoz, M. S. Hernández Pérez, F. Javier Jover Maestre, J. Lomba Maurandi, A. Avilés Fernández, K. T. Lillios, A. M. Silva, M. Magalhães Ramalho, L. M. Oosterbeek, C. Cunha, A. J. Waterman,

J. Roig Buxó, A. Martínez, J. Ponce Martínez, M. Hunt Ortiz, J. C. Mejías-García, J. C. Pecero Espín, R. Cruz-Auñón Briones, T. Tomé, E. Carmona Ballesteros, J. L. Cardoso, A. C. Araújo, C. Liesau von Lettow-Vorbeck, C. Blasco Bosqued, P. Ríos Mendoza, R.-G. Pujante A, J. I. M. A. Esquembre Beviá, V. M. Dos Santos Goncalves, R. Parreira, E. Morán Hernández, E. Méndez Izquierdo, J. Vega de Miguel, R. Menduiña García, V. Martínez Calvo, O. López Jiménez, J. Krause, S. L. Pichler, R. Garrido-Peña, M. Kunst, R. Risch, M. A. Rojo-Guerra, W. Haak, and K. W. Alt, “The maternal genetic make-up of the Iberian Peninsula between the Neolithic and the Early Bronze Age,” *Scientific Reports*, 7, 15644 (2017).

[17] D. H. Ubelaker, [Human skeletal remains: excavation, analysis, interpretation] Taraxacum, Washington(1989).

[18] F. J. Rühli, N. Nicklisch, and K. W. Alt, “A historical case of beaten-copper cranium,” *Journal of Neurosurgery*, 106, 71-73 (2007).

[19] B. Müller, F. Beckmann, M. Huser, F. Maspero, G. Szekely, K. Ruffieux, P. Thurner, and E. Wintermantel, “Non-destructive three-dimensional evaluation of a polymer sponge by micro-tomography using synchrotron radiation,” *Biomolecular Engineering*, 19, 73-78 (2002).